APS physics

CHORUS

This is the accepted manuscript made available via CHORUS. The article has been published as:

Carrier dynamics in femtosecond-laser-excited bismuth telluride

J. L. Wang, L. Guo, C. Ling, Y. M. Song, X. F. Xu, Z. H. Ni, and Y. F. Chen

Phys. Rev. B **93**, 155306 — Published 28 April 2016

DOI: 10.1103/PhysRevB.93.155306

Carrier Dynamics in Femtosecond-Laser-Excited Bismuth Telluride

J. L. Wang,[1,*] L. Guo,[2] C. Ling,[1] Y. M. Song,[1] X. F. Xu,[2,*] Z. H. Ni, [1] and Y. F. Chen[1]

[1] Jiangsu Key Laboratory for Design and Manufacture of Micro/Nano Biomedical Instruments, Southeast University, Nanjing 210096, China

[2] School of Mechanical Engineering and Birck Nanotechnology Center, Purdue University, West Lafayette, Indiana 47907, USA

[*] Correspondence: xxu@ecn.purdue.edu (X. X.), wangjianli@seu.edu.cn (J. W.)

The carrier dynamics of Bi_2Te_3 is studied using the femtosecond pump-probe technique. Three distinct processes, including free carrier absorption, band filling and electron-hole recombination, are found to contribute to the reflectivity changes. The two temperature model is used to describe the intraband energy relaxation process of carriers, and the Drude contribution well explains the intensity dependence of the peak values of the non-oscillatory component in the reflectivity signal. The combined effects of free carrier absorption and band filling result in a reflection minimum at about 2 ps after the laser excitation. The non-zero background signal increases linearly with the pump fluence, which is attributed to the electron-hole recombination. Finally, our results provide an illustration of investigating the carrier dynamics in semiconductors from the ultrafast reflectivity spectra.

I. INTRODUCTION

Bismuth-based semiconductors, such as Bi_2Te_3 and Bi_2Se_3, have attracted intense interests due to their importance in applications as thermoelectric materials [1] and in fundamental physics as topological insulators [2]. Using ultrafast pump-probe spectroscopy, the carrier dynamics in these materials have been extensively studied. In general, the time-resolved reflectivity is comprised of both damped oscillatory and non-oscillatory components [3], which can be attributed to the dynamics of coherent optical phonons [4,5] and the dynamics of carriers and incoherent phonons, respectively. Despite rich experimental and theoretical investigations, the explanation for the reflectivity trace, especially for the non-oscillatory part, is still lack of consistency due to the complex dynamics of carriers and phonons after optical excitation.

Multiple exponential decay functions have been widely used to fit the transient reflectivity traces, and the different carrier dynamics are proposed to feature different characteristic times [6-14]. These phenomenological models can fit the experimental data well, but are not sufficient to reveal the underlying mechanisms. For instance, both positive and negative amplitudes are observed in the non-oscillatory part of the transient reflectivity signals in Bi_2Se_3 [8], Bi [10] and Bi_2Te_3 [13, 14], and the electron-phonon interactions and trapping of electrons were speculated as the reasons of the positive and negative terms, respectively. The terms associated with lattice heating were sometimes discussed [10, 13], but the effect of lattice heating on reflectivity is not fully understood. Moreover, a pronounced dip at around 2 to 8 ps after the pump excitation has been widely observed [8, 12,13,15], but its origin is unknown [15].

With a large amount of electrons excited from the valence band to the conduction band by the pump laser, the change in the dielectric constant reflects the change of the probability of intraband

and interband transitions. The intraband effect is similar to what usually occurs in metals, which reflects the coupling between hot carriers and phonons. The interband effect can arise from band filling, bandgap shrinkage and electron-hole recombination [16]. Making simplifications of band structures, some attempts have been made to combine different processes to interpret the change in the dielectric constant [16-18]. For the direct-gap semiconductor, Bennett et al [16] proposed a model to describe the band filling effect. Considering the change in the real part of the refractive index, Sabbah and Riffle [17] deduced an expression for the contribution from the free carrier absorption. Using the similar models, Guo et al [19] decoupled the contributions from intraband and interband transitions by tuning the probe wavelength. However, for the bismuth-based semiconductors, the imaginary part and real part in the refractive index are comparable [20], therefore, the simplified model for free carrier absorption may be inappropriate. Since the reflectivity spectra have been used to evaluate the energy band structure of semiconductors [20], using the established relations between the reflectivity and the dielectric constant, we can probably improve the understanding of the carrier dynamics in the bismuth-based semiconductors.

In this work, the Drude-Lorentz model is used to describe the far-infrared reflectivity spectra of Bi_2Te_3, the two temperature model (TTM) accounts for the interaction between hot carriers and phonons in the conduction band, and the effects of free carrier absorption, band filling and electron-hole recombination are included to evaluate the time-resolved reflectivity at a fix probe wavelength. This approach is subsequently employed to provide an understanding of the transient reflectivity change as a function of the pump fluence.

II. EXPERIMENTAL

In this experiment, p-type Bi_2Te_3 single crystalline films with thickness of 50nm were

synthesized by metalorganic chemical vapor deposition on a (100) GaAs substrate. The reflectivity change was detected using a standard two-color (400 and 800 nm) pump-probe layout [14, 21]. The femtosecond laser pulse with central wavelength at 800 nm was generated by an amplifier system at a repetition rate of 5 kHz. The beam from the amplifier was split into a pump pulse and a probe pulse. A half wave plate and a polarizer were installed in the pump beam to control the intensity, and a second harmonic crystal was used to convert the 800 nm pump pulses into 400 nm pulses. The pump beam was then modulated by a mechanical chopper at a frequency of 500 Hz. The time delay between the probe and the pump beams was controlled by a mechanical delay stage installed in the probe arm. The collinear pump and probe beams were focused onto the sample surface with spot diameters of about 80 μm and 20 μm, respectively. Finally, the reflectivity changes of the probe beam were measured by a balanced detector and a lock-in amplifier.

III. THEORETICAL MODELS

Figure 1a shows a typical reflectivity signal of Bi_2Te_3 film measured at room temperature with a pump fluence of 0.28 mJ/cm^2. The main features obtained from various pump fluences are similar to the data shown in this figure. The photoinduced response of Bi_2Te_3 can be represented by the following expression [3]

$$\frac{\Delta R}{R} = A_{\mathrm{op}} e^{-t/t_{\mathrm{op}}} \cos\left(2\pi f t + \varphi\right) + \left(\frac{\Delta R}{R}\right)_{\mathrm{non}} \qquad (1)$$

The oscillation is caused by the damped A_{1g} coherent optical phonons [4,5]. The frequency, f, is about 1.87 THz, which is closed to the value obtained from Raman spectroscopy (1.88 THz [22]). The dephasing time, t_{op}, is about 5 ps, which is also consistent with the reported data [4,5,9].

For the non-oscillation part, we observe a sharp decrease in reflectivity, followed by a fast

rise. After a dip at about 2 ps, the reflectivity decreases again to reach a plateau at around 15 ps, and finally increases slowly to a non-zero background within the time frame of the measurement. To interpret the rich phenomena, we refer to the reflectivity spectra. The reflectivity can be calculated by

$$R = \left| \frac{1-\sqrt{\varepsilon_1 + i\varepsilon_2}}{1+\sqrt{\varepsilon_1 + i\varepsilon_2}} \right|^2 \tag{2}$$

where $\varepsilon=\varepsilon_1+i\varepsilon_2$ is the complex dielectric constant. When the pump pulse is incident upon a semiconductor and the corresponding dielectric constant can be described by the Drude-Lorentz model [23]

$$\varepsilon = \varepsilon_1 + i\varepsilon_2 = 1 - \frac{{\omega_p}^2}{\omega^2 + i\omega\gamma_{ep}} + \sum_j \frac{{\omega_{pj}}^2}{{\omega_{0j}}^2 - \omega^2 - i\omega\gamma_j} \tag{3}$$

where the second term on the right side is the Drude contribution due to free carrier intraband absorption, ω_p is the plasma frequency of free carriers, which is a function of carrier density, γ_{ep} is the carrier damping rate (ps^{-1}), and ω is the frequency of the probe pulse. The third term stands for the contribution of interband transition and has the form of multiple Lorentzian oscillators, and ω_{pj}, ω_{0j} and γ_j are the plasma frequency, resonant frequency and damping rate of each oscillator j. To decouple the intraband and interband effects, we refer to the reflectance spectra of Bi_2Te_3 in the far-infrared region. For simplicity, only single Lorentzian oscillator is considered, and the best-fitting values are ω_{01}=5454.4 cm^{-1}, ω_{p1}=49755 cm^{-1}, and γ_1=6586.9 cm^{-1}. The obtained reflectivity spectra is shown in Fig 2, which agrees well with the experimental data [23]. It demonstrates that, when the frequency is less than 500 cm^{-1}, the Drude contribution dominates the complex dielectric constant ε, and the effect of interband transition increases as frequency increases. For frequencies larger than 1000 cm^{-1}, both interband and intraband should be taken

into consideration. In our subsequent analysis, the parameters associated with the interband transition are maintained the same, while the Drude components (ω_p and γ_{ep}) are different from the data fitted from the reflectivity in the far-infrared region due to different carrier density.

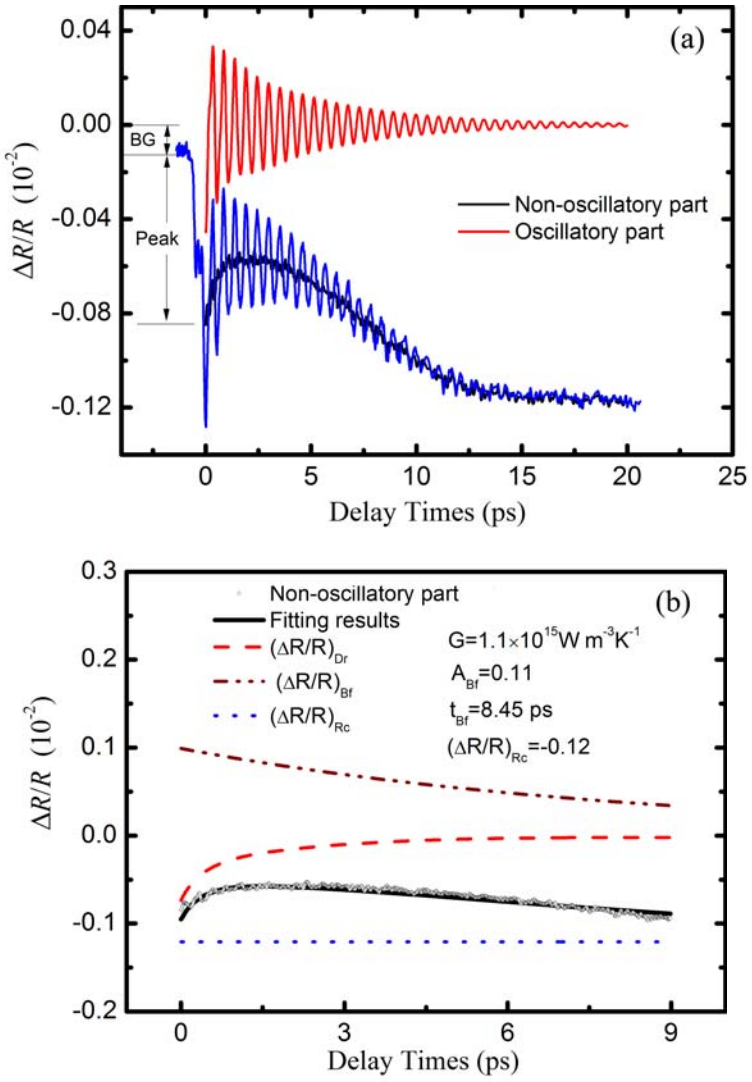

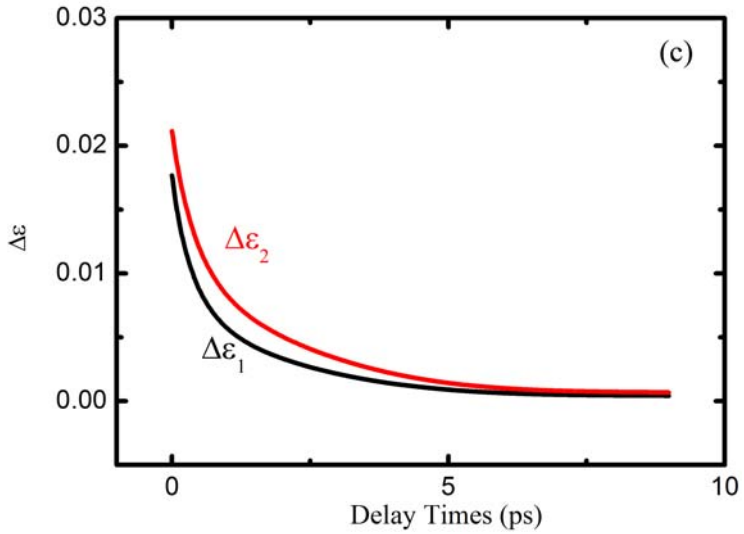

FIG. 1. (a) Time-resolved reflectivity of Bi_2Te_3 excited at 0.28 mJ/cm^2, together with the non-zero background signal and the peak value of the non-oscillatory component. (b) The best-fit results (the dark solid line) calculted by Eq. (4) combined with the contributions from free carrier absorption, band filling and electron-hole recombination. (c) The changes in dielectric constant solely attributed to the Drude contribution.

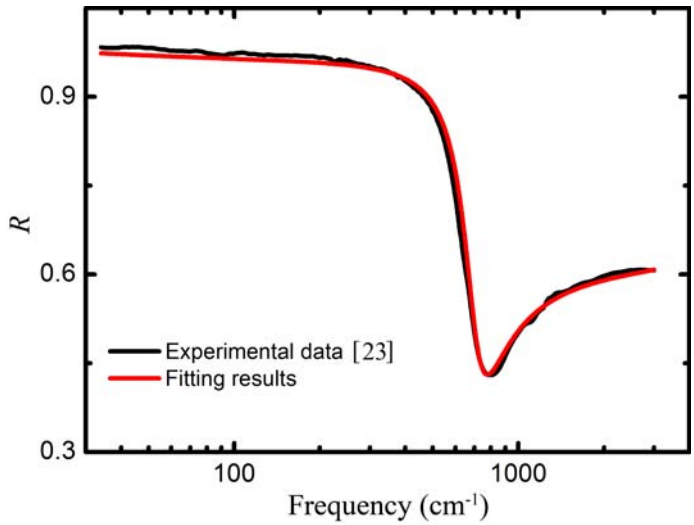

FIG. 2. Reflectivity spectra of Bi_2Te_3 in the far-infrared region fitted by the Drude-Lorentz model (the red solid line).

If the contributions from the interband transition arise from band filling and electron-hole recombination, the change in non-oscillatory reflectivity can be expressed by

$$\left(\frac{\Delta R}{R}\right)_{\text{non}} = \left(\frac{\Delta R}{R}\right)_{\text{Dr}} + \left(\frac{\Delta R}{R}\right)_{\text{Bf}} + \left(\frac{\Delta R}{R}\right)_{\text{Rc}} \tag{4}$$

The subscripts Dr, Bf, and Rc account for the contributions from the free carrier absorption, band filling effect and electron-hole recombination, respectively. The non-zero background (BG) signal before the arrival of pump pulse indicates that the relaxation time of the electron-hole recombination process is larger than the pulse interval (0.2 ms), so $(\Delta R/R)_{\text{Rc}}$ is a constant value taking into account the time frame of 20 ps (Figure 1a).

The Drude model is used to relate the electron temperature T_e and the lattice temperature T_p to the dielectric function by the damping rate γ_{ep}, which can be expressed as

$$\gamma_{ep} = A_{ee}T_e^2 + B_{ep}T_p \tag{5}$$

The initial reflectivity can be calculated from Eqs. (2) and (3), when $T_e = T_p = 300$ K. After the laser excitation, the change in reflectivity, $(\Delta R/R)_{\text{Dr}}$, is mainly caused by the change in γ_{ep}, and the temporal evolution of electron and lattice temperatures can be simulated by the TTM as follows

$$C_{e0}T_e\frac{\partial T_e}{\partial t} = \lambda_e\frac{\partial^2 T_e}{\partial x^2} - G\left(T_e - T_p\right) + \frac{0.94(1-R)F}{t_p\delta}\exp\left[-\frac{x}{\delta} - 4\ln 2\left(\frac{t}{t_p}\right)^2\right] \tag{6}$$

$$C_p\frac{\partial T_p}{\partial t} = \lambda_p\frac{\partial^2 T_p}{\partial x^2} + G\left(T_e - T_p\right) \tag{7}$$

where the subscripts e and p denote electrons and phonons respectively, λ is the thermal conductivity, G is the electron-phonon coupling factor, indicating the energy transfer rate from

electrons to phonons, C_p is the volumetric specific heat capacity, F is the pump fluence, t_p is the pulse width, δ is the optical penetration depth (9.1 nm for 400 nm wavelength), L is the thickness of the Bi_2Te_3 film used in the experiment (L= 50 nm), C_{e0} is the electron specific heat coefficient, which is calculated by $C_{e0}=\pi^2 k_B^2 n_e/(2\varepsilon_F)$ [9], k_B is Boltzmann constant, n_e is the doping density, the Fermi energy is defined by $\varepsilon_F=\hbar^2(3\pi^2 n_e)^{2/3}/(2m)$, with electron mass m, and the reduced Planck constant $\hbar$.

When the electrons are excited from the valence band to the conduction band by the pump laser, the lower states in the conduction band are firstly filled. For the subsequent laser pulse, higher photon energy is needed to excite electrons into the conduction band, resulting in the decrease of absorption at the pump wavelength. This phenomenon has been explained by band filling [16]. The contribution from the band filling effect can be simplified by [19]

$$\left(\frac{\Delta R}{R}\right)_{Bf} = A_{Bf}\frac{erf(t/t_p)+1}{2}\exp(-\frac{t}{t_{Bf}}) \tag{8}$$

where A_{Bf} is the amplitude, erf is the error function, and t_{Bf} is the relaxation time. The sign of A_{Bf} can be analyzed as

$$\left(\frac{\Delta R}{R}\right)_{Bf} = \frac{1}{R}\left[\Delta\varepsilon_1\frac{\partial R}{\partial\varepsilon_1}+\Delta\varepsilon_2\frac{\partial R}{\partial\varepsilon_2}\right] \tag{9}$$

$$\frac{1}{R}\frac{\partial R}{\partial\varepsilon_1} = \frac{\left(2\varepsilon_1-|\varepsilon|-1\right)\sqrt{2\left(\varepsilon_1+|\varepsilon|\right)}}{|\varepsilon|\left[\left(\varepsilon_1-1\right)^2+\varepsilon_2^{\,2}\right]} \tag{10}$$

$$\frac{1}{R}\frac{\partial R}{\partial\varepsilon_2} = \frac{\sqrt{2}\varepsilon_2\left(2\varepsilon_1+|\varepsilon|-1\right)}{|\varepsilon|\sqrt{\varepsilon_1+|\varepsilon|}\left[\left(\varepsilon_1-1\right)^2+\varepsilon_2^{\,2}\right]} \tag{11}$$

Taking the complex reflective index to be $\varepsilon=\varepsilon_1+i\varepsilon_2$=-26.25+52$i$ (at 800 nm wavelength) [20], the reflectivity is calculated to be R=0.76, and $\partial R/\partial\varepsilon_1 \approx -3.4\times10^{-3}$ and $\partial R/\partial\varepsilon_2 \approx 2.3\times10^{-4}$. Due to band filling, the absorption decreases at the pump wavelength (400 nm), i.e., $\Delta\varepsilon_2<0$. Since probe

wavelength is longer than that of the pump laser but much shorter than the wavelength corresponding to the band gap (~9500nm), as analyzed in Guo et al, [19], $\Delta\varepsilon_1$ is inclined to be negative. $\Delta\varepsilon_2<0$ occurs only within a narrow spectrum, and the amplitude of $\partial R/\partial\varepsilon_2$ is one order smaller than $\partial R/\partial\varepsilon_1$, so $\Delta\varepsilon_1$ dominates the change in the reflectivity, and $(\Delta R/R)_{Bf}$ should be positive.

Figure 1b shows the non-oscillatory part of the reflectivity changes. The solid curve is calculated from Eq. (4), and shows a good fit. The contribution from each component (dashed lines) is also presented in this figure, and the temporal evolution of T_e and T_p is presented in Supplemental Material [24]. In the TTM simulation, λ_e=0.5 W m^{-1} K^{-1}[25], λ_p=1.7 W m^{-1} K^{-1}[25],C_p=1.21×10^6 J m^{-3} K^{-2} [26], n_e=1.16×10^{25} m^{-3} [27], so C_{e0} is calculated to be 3.6 J $m^{-3}K^{-2}$. A_{ee} and B_{ep} for Bi_2Te_3 are both unknown. Here, their values are assumed to be the same as Au, with A_{ee}=1.1×10^7 s^{-1} K^{-2} and B_{ep}=3.6×10^{11} s^{-1} K^{-1} [28], which are assumed to be independent of the excited carrier density. Therefore, the parameters including G, A_{Bf}, t_{Bf} and $(\Delta R/R)_{Rc}$ are obtained to best-fit the reflectivity trace, and their values are also listed in Fig. 1b. The fitted coupling factor G is about 10^{15} W m^{-3} K^{-1}, similar to the value in $Bi_{1.5}Sb_{0.5}Te_{1.8}Se_{1.2}$[12], but about one order smaller than that in metallic films. The amplitude of $(\Delta R/R)_{Bf}$ is positive according to the preceding analysis, while the Drude contribution is negative. Figure 1c shows the temporal evolution of $\Delta\varepsilon_1$ and $\Delta\varepsilon_2$ resulted from the Drude contribution. Similar to the analysis in band filling effect, $\Delta\varepsilon_1$ plays a dominant role in $\Delta R/R$, the positive $\Delta\varepsilon_1$ results in a negative $(\Delta R/R)_{Dr}$. As a consequence, the dip at about 2 ps can be interpreted as a competition between free carrier absorption and band filling effect. From the simulation results based on the TTM, after about 15 ps, thermal equilibrium between electrons and phonons is achieved. The Drude model shows that the

contribution from lattice heating (T_p) is relatively small, so we attributed the BG signal to the recombination of electrons and holes, which is further verified in analyzing the intensity-dependent reflectivity as described below.

III. DISCUSSIONS

Based on the theoretical model, we can re-examine the carrier dynamics as a function of pump fluence. The pump fluence varies from 0.45 to 2.7 mJ/cm^2, and the changes in reflectivity are shown in Fig. 3. Table I lists the fitting parameters. As illustrated in Bi_2Se_3 [6], the BG signal obtained here is found to increase linearly with the carrier density (pump fluence). The repetition rate is 5 kHz, applying the two-layer thermal diffusion model [29], we neglect the thermal accumulation effect (see the Supplemental Material [30]). The origin of the large decay time can be attributed to the recombination of holes and electrons through the mechanism of trapping [31]. The ratio of the BG signals to $(\Delta R/R)_{Rc}$ is used to estimate the recombination rate γ by supposing an exponential decay function as $e^{t\gamma}$ with t = 0.2 ms. The dependence of recombination rate, γ, upon the carrier density can be modelled by [31]

$$\gamma = \gamma_0 \frac{1 + cN_e}{1 + aN_e} \tag{12}$$

N_e is the excited carrier density, which is related with the pump fluence by $N_e=(1-R)F/(E_g\delta)$ [9], γ_0 is the recombination rate for small value of N_e, E_g is the energy band gap (0.13 eV [32]), and c and a are two parameters associated with the numbers of electrons and holes at equilibrium states and those calculated by virtual Fermi level, as well as the probabilities to capture a hole or an electron by traps [31]. Figure 4 shows the recombination rate decreases monotonically with the carrier density, the solid line is plotted to guide the eye with $a = 8\times10^{-21}$ cm^3 and $c = 2\times10^{-20}$ cm^3.

TABLE I. Fitting parameters

F (mJ/cm^2)	Oscillatory part			Non-oscillatory part					
	A_{op} (10^{-3})	t_{op} (ps)	f (THz)	BG (10^{-3})	Peak (10^{-3})	A_{Bf} (10^{-3})	t_{Bf} (ps)	G (10^{15} W m^{-3} K^{-1})	$(\Delta R/R)_{Rc}$ (10^{-3})
0.45	0.32	7.0	1.87	2.13	0.98	1.4	6.4	0.93	2.98
0.69	0.38	5.6	1.87	2.54	1.54	2.1	5.9	1.2	3.64
1.27	0.57	6.6	1.86	4.81	2.69	3.0	5.4	1.8	6.70
1.91	0.80	5.1	1.85	7.47	2.92	4.3	4.9	2.6	9.87
2.75	0.82	4.9	1.86	9.26	3.75	4.7	4.5	3.3	12.1

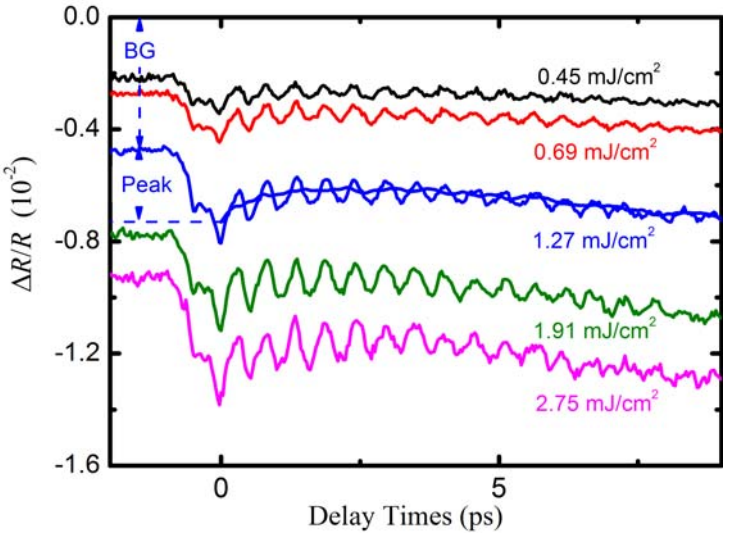

FIG. 3. The time-resolved reflectivity pumped by different laser fluences, the BG signal and peak value are exampled for the pump fluence of 1.27 mJ/cm^2.

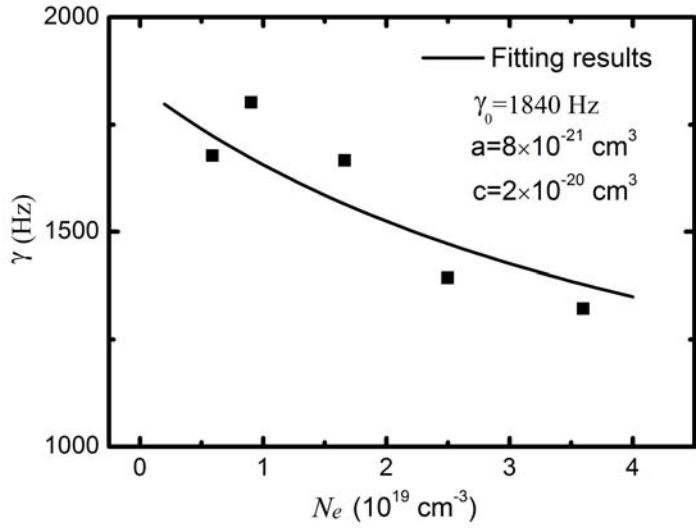

FIG. 4. Dependence of recombination rate upon the excited carrier density, the solid line shows the results calculated by Eq. (12)

Qualitatively, our results provide an evidence that the TTM is applicable in understanding the ultrafast energy transfer process in semiconductor, though some works argued that the TTM failed in the high-fluence regime [12] or at low temperature [33]. Here, the description of the intraband transition is based on the TTM, while the complex interband transition is simplified by an exponential decay function. Using the TTM combined with the Drude model, we can estimate the peak reflectivity values as a function of pump fluence as shown in Fig. 5. In this calculation, the maximum electron temperature is estimated by $T_{e,max}=[4\varepsilon_F\alpha F/\pi^2 N_e\delta]^{1/2}/k_B$ [9], the corresponding T_p stays at room temperature, and the Drude contribution is solely considered. It shows that, the calculated peak reflectivity decreases parabolically as fluence increases, which has a similar trend as the experimental data. Meanwhile, the fitted G is found to increase as fluence increases, together with the decreasing t_{Bf} and t_{op}. Small t_{op} corresponds to fast coupling between the coherent optical phonons and the acoustic phonons, indicating more efficient energy transport

from the hot carriers to the acoustic phonons, which can explain the intensity dependence of G and t_{Bf}. This coincidence further confirms that the correspondence exists between the dynamics of the coherent optical phonons and the hot carriers [14].

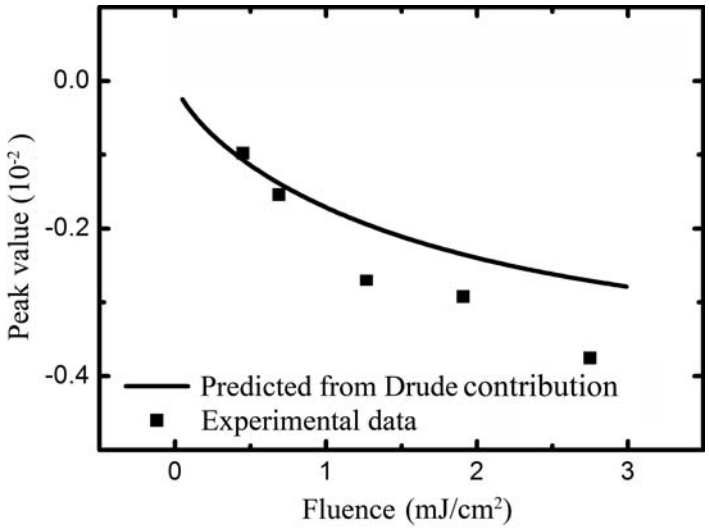

FIG. 5. Dependence of the peak value of the non-oscillatory component upon the pump fluence, the solid line demonstrates the contribution from free carrier absorption.

Here, we make a few comments concerning intraband and interband transitions. First, the carrier-phonon relaxation time can be estimated by [34]

$$\tau_{e-p}(t) = \frac{C_{e0}\left[T_e(t) + T_p(t)\right]}{2G} \tag{13}$$

For the pump fluence of 0.45 mJ/cm^2, the relaxation time is estimated by averaging the data within the time interval of 0 to 9 ps, which is found to be 2.8 ps, much larger than that obtained in metallic films, but is similar to the value corresponds to the carrier-acoustic-phonon interaction in Bi_2Se_3 [8]. Excluding this relatively slow relaxation term, to best-fit the experimental data using the multiple exponential decay functions, a fast decay component due to the carrier-optical-phonon interaction has been widely introduced [3, 8]. However, the present TTM

cannot directly include the effect of incoherent optical phonon, which is believed to mediate the carrier-phonon energy exchange. Therefore, it may be not sufficient to use a single *G* to describe the carrier-phonon interaction, and the TTM should be improved to take the incoherent optical phonon into consideration [35]. On the other hand, in this model, we simply assume that recombination occurs simultaneously with the other two effects, as demonstrated in Fig. 1b. The photon energy of pump and probe pulses are much larger than the energy band gap of Bi_2Te_3, and the interband transitions cause the occupation of different high energy states in the conduction band. If we refer to the energy band structure of Bi_2Te_3 suggested by Youn et al [36], the conduction minima and the valence band maxima are not located in the symmetry lines, which are more likely related to the recombination effect. As a consequence, delays may exist between carrier excitation and recombination, and the precise evaluation on the recombination effect in the ultrafast process is rather difficult. Though the phenomena of time-resolved reflectivity can be well interpreted using our model, all these above-mentioned factors are not included, which are beyond the scope of the present article.

IV. CONCLUSIONS

By considering the effects of intraband and interband transitions, we demonstrate that the rich phenomena can be revealed in the time-resolved reflectivity of Bi_2Te_3 film. The non-zero BG signals increase linearly with the pump fluence, which is believed to be caused by electron-hole recombination. The TTM is applied to describe the energy relaxation process of carriers in the conduction band. The opposite signs for the contribution from free carrier absorption and band filling are explained with the aid of the reflectivity spectra. The dip at around 2 ps reflects the competition among these effects. Finally, the coincidence between the electron-phonon coupling

factor and the relaxation time of coherent optical phonons indicates that the dynamics of the coherent optical phonons and the carriers are strongly coupled.

ACKNOWLEDGMENTS

The authors thank Dr. Rama Venkatasubramanian for preparing the films. This work was supported by the National Science of Foundation Award No. 1048616, the Department of Energy through a Corporate Agreement No. DE-AC05000OR22725 with General Motors R&D, the National Basic Research Programme of China (Grant No. 2011CB707605), and the National Natural Science Foundation of China (Grant No. 51476033).

[1] R. Venkatasubramanian, E. Siivola, T. Colpitts, and B. O'Quinn, Nature **413**, 597(2001).

[2] H.J. Zhang, C.X. Liu, X.L. Qi, X. Dai, Z. Fang, and S.C. Zhang, Nat Phys **5**, 438 (2009).

[3] A.A. Melnikov, O.V. Misochko, and S.V. Chekalin, J Appl Phys **114**, 033502 (2013).

[4] J. Flock, T. Dekorsy, and O.V. Misochko, Appl Phys Lett **105**, 011902 (2014).

[5]O.V. Misochko, J. Flock, and T. Dekorsy, Phys Rev B **91**, 174303 (2015).

[6] Y.D. Glinka, S. Babakiray, T.A. Johnson, A.D. Bristow, M.B. Holcomb, and D. Lederman, Appl Phys Lett **103**, 151903 (2013).

[7] P. Grenier, and J.F. Whitaker, Appl Phys Lett **70**, 1998 (1997).

[8] J. Qi, X. Chen, W. Yu, P. Cadden-Zimansky, D. Smirnov, N.H. Tolk, I. Miotkowski, H. Cao, Y.P. Chen, Y. Wu, S. Qiao, and Z. Jiang, Appl Phys Lett **97**, 182102 (2010).

[9] Y. Wang, L. Guo, X. Xu, J. Pierce, and R. Venkatasubramanian, Phys Rev B **88**, 064307 (2013).

[10] A.Q. Wu, and X. Xu, Appl Phys Lett **90**, 251111 (2007).

[11] Y. Xu, M. Khafizov, L. Satrapinsky, P. Kus, A. Plecenik, and R. Sobolewski, Phys Rev Lett **91**, 197004 (2003).

[12] L. Cheng, C. La-o-vorakiat, C.S. Tang, S.K. Nair, B. Xia, L. Wang, J.-X. Zhu, and E.E.M. Chia, Appl Phys Lett **104**, 211906 (2014).

[13] L. Jia, W. Ma, and X. Zhang, Appl Phys Lett **104**, 241911(2014).

[14] J.L. Wang, L. Guo, C.H. Liu, X. Xu, and Y.F. Chen, Appl Phys Lett **107**, 063107 (2015).

[15] N. Kumar, B.A. Ruzicka, N.P. Butch, P. Syers, K. Kirshenbaum, J. Paglione, and H. Zhao, Phys Rev B **83**, 235306 (2011).

[16] B.R. Bennett, R.A. Soref, and J.A. Delalamo, IEEE J Quantum Elect **26**, 113(1990).

[17] A.J. Sabbah, and D.M. Riffe, Phys Rev B **66**, 165217 (2002).

[18] M.A.M. Versteegh, T. Kuis, H.T.C. Stoof, and J.I. Dijkhuis, Phys Rev B **84**, 035207 (2011).

[19] L. Guo, X.F. Xu, and J.R. Salvador, Appl Phys Lett **106**, 231902 (2015).

[20] Greenawa.Dl, and G. Harbeke, J Phys Chem Solids **26**, 1585(1965).

[21] A.Q. Wu, X. Xu, and R. Venkatasubramanian, Appl Phys Lett **92**, 011108 (2008).

[22] W. Richter, and C.R. Becker, Phys Status Solidi B **84**, 619(1977).

[23] M.S. Wolf, Infrared and Optical Studies of Topological Insulators Bi_2Te_3, Bi_2Se_3, and Sb_2Te_3, Ph.D thesis, University of Akron, 2011.

[24] See Supplemental Material at URL for details of calculation.

[25] H.J. Goldsmid, Proc Phys Soc Lond B **69**, 203 (1956).

[26] N.P. Gorbachuk, A.S. Bolgar, V.R. Sidorko, and L.V. Goncharuk, Powder Metall Met Ceramics **43**, 284 (2004).

[27] A.Q.Wu, Ultrafast Dynamics of Coherent Phonon Vibration in Thermoelectric Materials, Ph.D thesis, Purdue University, 2008.

[28] P.E. Hopkins, Phys Rev B **81**, 035413 (2010).

[29] A.J. Schmidt, X. Chen, and G. Chen, Rev Sci Instrum **79**, 114902 (2008).

[30] See Supplemental Material at URL for details of calculations and discussions.

[31] W. Shockley, and W.T. Read, Phys Rev **87**, 835 (1952).

[32] I.G. Austin, Proc Phys Soc London **72**, 545 (1958).

[33] Y.P. Lai, H.J. Chen, K.H. Wu, and J.M. Liu, Appl Phys Lett **105**, 232110 (2014).

[34] R.H.M. Groeneveld, R. Sprik, and A. Lagendijk, Phys Rev B **51**, 11433 (1995).

[35] H.M. van Driel, Phys Rev B **19**, 5928 (1979).

[36] S.J. Youn, and A.J. Freeman, Phys Rev B **63**, 085112 (2001).

TABLE I. Fitting parameters

	Oscillatory part				Non-oscillatory part				
F (mJ/cm^2)	A_{op} (10^{-3})	t_{op} (ps)	f (THz)	BG (10^{-3})	Peak (10^{-3})	A_{Bf} (10^{-3})	t_{Bf} (ps)	G (10^{15} W m^{-3} K^{-1})	$(\Delta R/R)_{Rc}$ (10^{-3})
0.45	0.32	7.0	1.87	2.13	0.98	1.4	6.4	0.93	2.98
0.69	0.38	5.6	1.87	2.54	1.54	2.1	5.9	1.2	3.64
1.27	0.57	6.6	1.86	4.81	2.69	3.0	5.4	1.8	6.70
1.91	0.80	5.1	1.85	7.47	2.92	4.3	4.9	2.6	9.87
2.75	0.82	4.9	1.86	9.26	3.75	4.7	4.5	3.3	12.1

Figure Captions

FIG. 1. (a) Time-resolved reflectivity of Bi_2Te_3 excited at 0.28 mJ/cm^2, together with the non-zero background signal and the peak value of the non-oscillatory component. (b) The best-fit results (the dark solid line) calculted by Eq. (4) combined with the contributions from free carrier absorption, band filling and electron-hole recombination. (c) The changes in dielectric constant solely attributed to the Drude contribution.

FIG. 2. Reflectivity spectra of Bi_2Te_3 in the far-infrared region fitted by the Drude-Lorentz model (the red solid line).

FIG. 3. The time-resolved reflectivity pumped by different laser fluence, the BG signal and peak value are exampled for the pump fluence of 1.27 mJ/cm^2.

FIG. 4. Dependence of recombination rate upon the excited carrier density, the solid line shows the results calculated by Eq. (12)

FIG. 5. Dependence of the peak value of the non-oscillatory component upon the pump fluence, the solid line demonstrates the contribution from free carrier absorption.